

Commensurate and Incommensurate Vortex States Confined in Mesoscopic Triangles of Weak Pinning Superconducting Thin Films

Nobuhito Kokubo^{1*}, Hajime Miyahara¹, Satoru Okayasu², and Tsutomu Nojima³

¹*Department of Engineering Science, University of Electro-Communications, Tokyo 182-8585, Japan*

²*Advanced Science Research Center, Japan Atomic Energy Agency, Ibaraki 319-1195, Japan*

³*Institute for Materials Research, Tohoku University, Sendai 980-8577, Japan*

We report on the direct observation of vortex states confined in equilateral and isosceles triangular dots of weak pinning amorphous superconducting thin films with a scanning superconducting quantum interference device microscope. The observed images illustrate not only pieces of a triangular vortex lattice as commensurate vortex states, but also incommensurate vortex states including metastable ones. We comparatively analyze vortex configurations found in different sample geometries and discuss the symmetry and stability of commensurate and incommensurate vortex configurations against deformations of the sample shape.

The concept of a small number of interacting particles in lateral confinement is found in a variety of physical systems, including electrons confined in semiconductor quantum dots,¹ electron dimples in the liquid-helium surface,² and paramagnetic colloids in cavities.³ Of particular interest is vortex matter in mesoscopic superconductors with different shapes.⁴⁻⁷ In addition to the vortex-vortex repulsion, vortices are subject to the lateral confinement due to the shielding current flowing along the sample boundary. The interplay between the inter-vortex interaction and the confinement results in unique vortex states with strong features of the sample shape, different from the Abrikosov-triangular lattice in bulk superconductors.⁸ It is well established that in mesoscopic disks, vortices form circular symmetric shells and obey the specific rules for shell filling with increasing the vorticity L .^{9,10} Meanwhile, in other geometric shapes such as squares¹¹⁻¹³ and pentagons,¹⁴ the formation of vortex shells is not well defined as in disks owing to the commensurability between the geometry and the vortex arrangement. In mesoscopic triangles, which we focus on this study, vortices form intrinsically a piece of the triangular lattice since they match the geometric shape with threefold

*E-mail: kokubo@pc.uec.ac.jp

axial symmetry.¹⁵ This occurs when vorticity becomes a triangular number, $L = n(n + 1)/2$ with integer n . For other vorticities, the formation of the triangular arrangement is not stable. Self-organized unique vortex patterns are formed.¹⁶ The corresponding vortex configurations are numerically proposed to have twofold (middle-plane reflection) symmetry and also to be represented by the combination of vortex “bricks”, i.e., lower vorticity configurations plus linear vortex chains.¹⁷

The visualization of vortex states in triangular dots was initiated by a scanning superconducting quantum-interference device (SQUID) microscopy study,¹⁸ followed by Bitter decoration studies.^{16,19} Both studies revealed some features dominated by inevitable inhomogeneity (pinning sites for vortices) in samples (Nb films). To observe vortex configurations inherent in mesoscopic triangles, it is crucial to use nearly pin-free, weak pinning materials such as amorphous superconducting films.^{13,20} In this work, we report on the direct observation of vortices confined in triangular dots of weak pinning amorphous MoGe films with the scanning SQUID microscope. Unlike the previous experimental studies that were limited to dots with the regular triangle shape,^{16,18} we further use isosceles triangular dots to obtain a better understanding of the commensurability effect(s), and study the symmetry and stability of commensurate and incommensurate vortex configurations against deformations of the sample shape.

We used a commercial scanning SQUID microscope (SQM-2000, SII Nanotechnology) with a dc SQUID magnetometer composed of Nb-based Josephson junctions and an inductively coupled, pick-up Nb coil of 10 μm diameter integrated on a small Si chip.¹⁸ The spatial resolution of the microscope is $\sim 4 \mu\text{m}$. The sample space is surrounded by a μ -metal shield, resulting in a residual magnetic field (ambient field) of $\sim 1.2 \mu\text{T}$. The details are described in Ref. 18.

Amorphous (α -)Mo_xGe_{1-x} ($x \approx 78$) films with thickness $d = 0.20 \mu\text{m}$ were deposited on Si substrates by rf-magnetron sputtering.²⁰ The superconducting transition temperature T_c is $\approx 7 \text{ K}$, the coherence length at zero temperature $T = 0$ is $\approx 5 \text{ nm}$, and the magnetic penetration depth $\lambda(0)$ at $T = 0$ is $\approx 0.6 \mu\text{m}$. Since the films are thinner than $\lambda(0)$, the screening of the supercurrent is characterized by the effective penetration depth [$\Lambda = 2\lambda^2/d \gg \lambda(0)$] and the interaction between vortices becomes long-ranged.²¹ Using standard photolithographic and wet-etching techniques, we fabricated isosceles triangular dots of two different shapes, together with equilateral triangular ones, as shown in Fig. 1. The isosceles triangular A dots have a height expanded by 20% with respect to the regular triangle, i.e., the ratio of the height b with respect to its base a is $b/a = 1.04$. The other B dots have a height reduced by

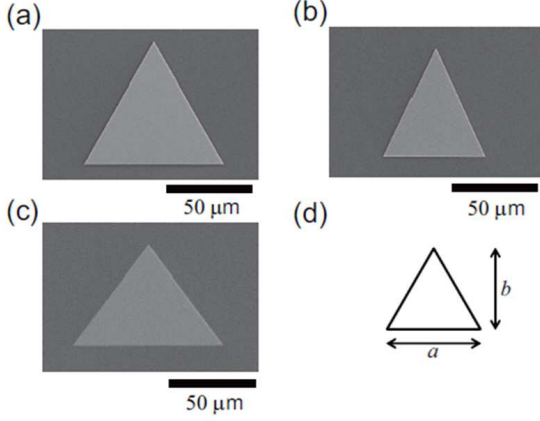


Fig. 1. Fig. 1. Electron micrographs of triangular dots of amorphous MoGe thin films. In addition to (a) equilateral triangular dots, we made isosceles triangular dots of two different shapes. (b) One (A) has a height expanded by 20% with respect to the regular triangle, i.e., the ratio of the height b with respect to its base a is $b/a = 1.04$. (c) The other (B) has a height reduced by 20%, i.e., $b/a = 0.69$.

20%, i.e., $b/a = 0.69$. We paid careful attention to the selection of the dots to avoid vortex configurations induced by pinning sites.¹³ We carried out a field-cooling procedure for every SQUID measurement to obtain an equilibrium vortex state.^{20,22}

Figures 2(a)–2(l) show vortex images in a $75\ \mu\text{m}$ equilateral triangular dot for vorticities $L = 1$ –11 observed after the dot was cooled to 3.7 K under different magnetic fields. Each image shows an area of $90 \times 90\ \mu\text{m}^2$ in size. A color bar indicates the magnitude of the magnetic flux per pixel of $3 \times 3\ \mu\text{m}^2$ normalized by the magnetic flux quantum Φ_0 . The corresponding traces of the vortex patterns are given in Figs. 2(m)–2(x). One can see the formation of pieces of the triangular lattice at triangular numbers of vorticities $L = 3$ [Fig. 2(d)], 6 [Fig. 2(g)], and 10 [Fig. 2(k)]. These configurations, together with a $L = 1$ configuration, are commensurate with the triangular dot geometry and have the threefold rotational symmetry with respect to the triangular dot center. We also observe a commensurate configuration at a nontriangular number of vorticity, $L = 4$. As shown in Figs. 2(e) and 2(q), a vortex appears in the dot center and the other three vortices form a triangle. Namely, commensurate patterns of $L = 1$ and 3 are combined. We note that this is the only case, and no other combination of commensurate patterns is observed up to $L = 11$.

For other nontriangular numbers of vorticities, we find incommensurate vortex states with configurations that are frustrated with the dot geometry. At $L = 2$ [Figs. 2(b) and 2(c)], vortices form a pair, but the pair orientation is rotatable in the dot. Focusing on three axes of symmetry in the triangular dot, we find that the observed orientations can be separated

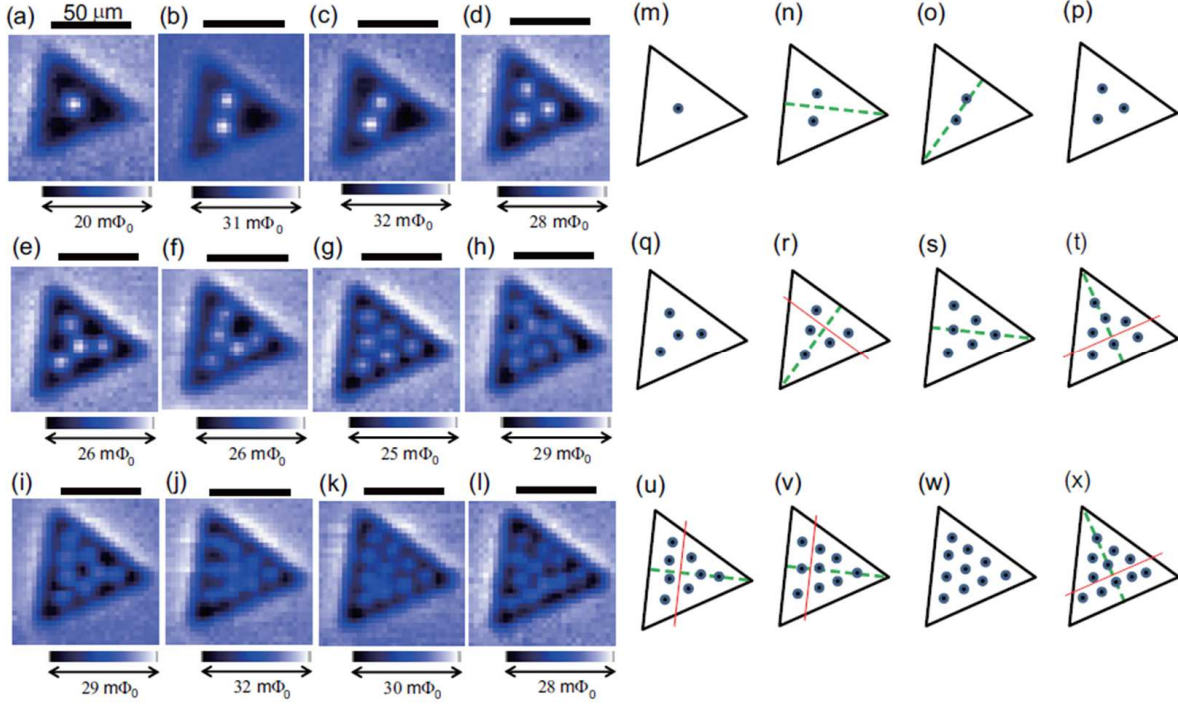


Fig. 2. Fig. 2. Scanning SQUID microscopy images of vortices in a $75 \mu\text{m}$ equilateral triangular dot for vorticities $L = 1$ – 11 observed after the dot was cooled to 3.7 K at different magnetic (coil) fields of (a) 5.0 , (b) 5.5 , (c) 6.5 , (d) 8.0 , (e) 9.3 , (f) 10 , (g) 11.5 , (h) 13 , (i) 14 , (j) 15 , (k) 17 , and (l) $18 \mu\text{T}$. All images are of areas of the same size ($90 \times 90 \mu\text{m}^2$). A color bar indicates the magnitude of the magnetic flux per pixel of $3 \times 3 \mu\text{m}^2$ normalized by the magnetic flux quantum Φ_0 . The traced vortex patterns are given in (m)–(x). The broken lines represent symmetry axes of the triangular dot. The solid lines are guides for the eyes.

into two. One is characterized by the orientation parallel to one of three symmetry axes, as represented by a broken line in Fig. 2(o). The other is perpendicular orientation, as shown in Fig. 2(n). As discussed later, these two pair states are intrinsic to the triangular dot, not induced by pinning sites.

At $L = 5$ [Fig. 2(f)], vortices are aligned parallel to the edges of the triangular dot and they form a V-shaped pattern. The observed configuration is nearly symmetric with respect to one of three symmetry axes in the triangular dot, as shown in the corresponding traced pattern [Fig. 2(r)]. It is interesting to note that this pattern can be divided into two: one is a commensurate triangular pattern and the other is a linear chain of two vortices. Other frustrated configurations at $L = 7$ – 9 and 11 are also explainable in terms of the combination of a commensurate vortex pattern and a linear vortex chain. The observed configurations (except for the perpendicular orientation of a vortex pair at $L = 2$) are in excellent agreement with the lowest-energy (ground) state configurations found in the numerical simulation.¹⁷

Table I. Vortex configurations observed in equilateral and isosceles triangular dots.

L	Configuration		
	Equilateral Triangle	Isosceles Triangle A	Isosceles Triangle B
1	$c1$	“ $c1$ ”	“ $c1$ ”
2	$l2_{//}, l2_{\perp}$	$l2_{//}$	$l2_{\perp}$
3	$c3$	“ $c3$ ”	“ $c3$ ”
4	$c4$	“ $c4$ ”	“ $c4$ ”
5	$c3 + l2$	“ $c3$ ” + $l2$	$l2 + l3$
6	$c6$	“ $c6$ ”	“ $c6$ ”
7	$c4 + l3, c3 + l4$	“ $c4$ ” + $l3$	“ $c3$ ” + $l4$
8	$c4 + l4$	“ $c3$ ” + $l2 + l3$	“ $c4$ ” + $l4$
9	$c6 + l3$	“ $c6$ ” + $l3$	$l2 + l3 + l4$
10	$c10$	“ $c10$ ”	“ $c10$ ”
11	$c6 + l5$	“ $c4$ ” + $l3 + l4$	“ $c6$ ” + $l5$

We summarize the observed vortex configurations for $L = 1$ – 11 in Table I using the notation for vortex configurations proposed in Ref. 17. The $L = 5$ state, for instance, can be denoted as $c3 + l2$, where $c3$ represents a commensurate $L = 3$ pattern and $l2$ denotes a linear chain of two vortices. Other incommensurate configurations can also be characterized by this nomenclature. In most cases, each L is characterized by the ground-state configuration. However, at $L = 7$, we occasionally observe a *metastable* $c3 + l4$ configuration in addition to a $c4 + l3$ configuration. Namely, the ground and metastable states are observable (or nearly degenerated) at $L = 7$. The situation is similar to that for $L = 2$ where two pair orientations appear. For distinction, we add subscript “ $//$ ” or “ \perp ” for the parallel or perpendicular orientation, respectively. The $l2_{//}$ configuration is numerically shown to be the ground state,^{16,17} suggesting the other ($l2_{\perp}$) to be a metastable state.

We would like to emphasize that all the frustrated vortex configurations observed in incommensurate states are characterized roughly by the reflection symmetry with respect to one of three symmetry axes in the triangular dot, in contrast to the threefold rotational symmetry in commensurate states. The appearance of the twofold symmetry in incommensurate states has also been shown numerically;¹⁷ however, the physical reason for the symmetry is not obvious and requires further investigation. In the following sections, we focus on the fact that the twofold symmetry is the characteristic one of isosceles triangles, and study whether the observed configurations appear in isosceles triangular dots of two different shapes (isosceles

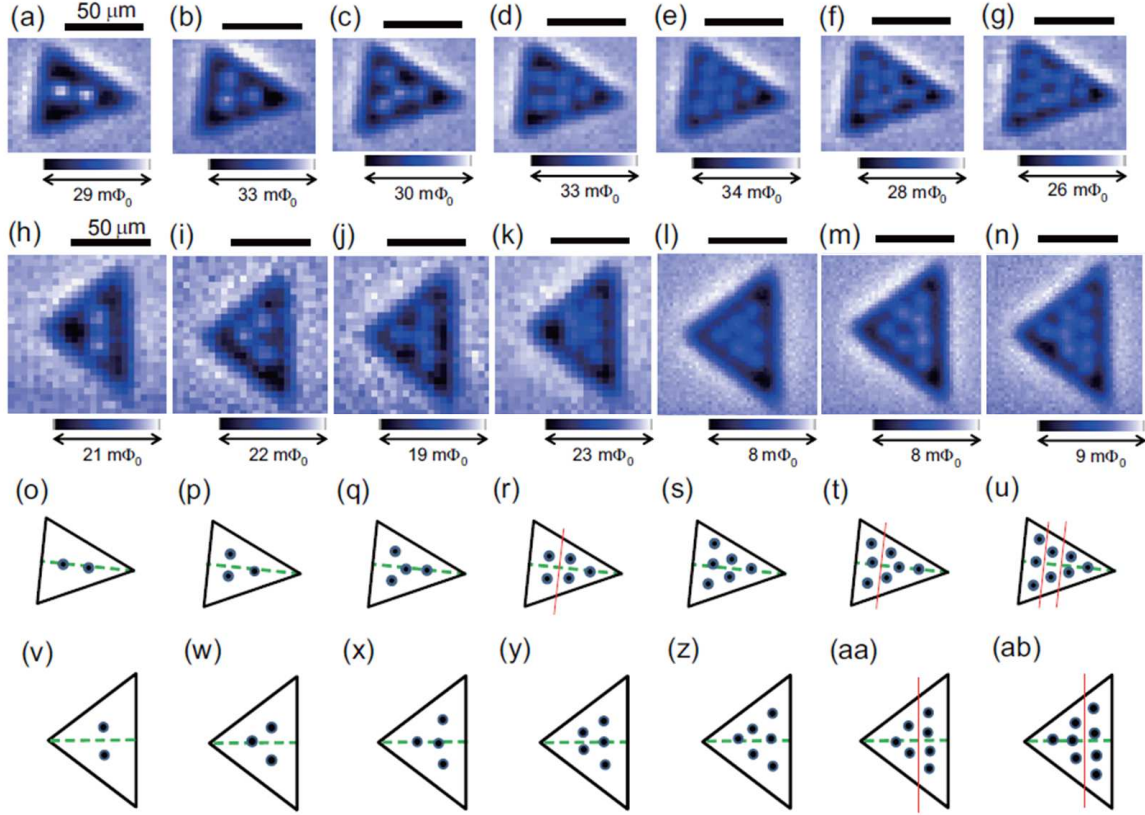


Fig. 3. Fig. 3. SQUID images of vortices in an isosceles triangular A dot with $60 \mu\text{m}$ base for $L = 2-8$ observed after cooling to 3.6 K at different magnetic (coil) fields of (a) 8.0 , (b) 10 , (c) 12 , (d) 14 , (e) 15 , (f) 16 , and (g) $17 \mu\text{T}$. These images are of areas of the same size of $90 \times 72 \mu\text{m}^2$. A color bar indicates the magnitude of the magnetic flux per pixel size of $3 \times 3 \mu\text{m}^2$ normalized by Φ_0 . The traced vortex patterns corresponding to the images in (a)–(g) are given in (o)–(u), respectively. We also present SQUID images observed in an isosceles triangular B dot with $90 \mu\text{m}$ base after cooling to 2.7 K at different fields of (h) 2.0 , (i) 2.5 , (j) 3.0 , (k) 3.8 , (l) 4.5 , (m) 4.8 , and (n) $5.0 \mu\text{T}$. These images are also of areas of the same size of $100 \times 100 \mu\text{m}^2$. A color bar indicates the magnitude of the magnetic flux per pixel size of $4 \times 4 \mu\text{m}^2$ for (h)–(k), and that of $2 \times 2 \mu\text{m}^2$ for (l)–(n). The traced patterns corresponding to the images in (h)–(n) are given in (v)–(ab), respectively.

A and B dots).

Selected images observed in isosceles A and B dots are given in Figs. 3(a)–3(g) and 3(h)–3(n), respectively. As traced in Figs. 3(o)–3(ab), all the vortex configurations are found to have the twofold reflection symmetry with respect to the symmetry axis of isosceles triangular dots. From the comparison of vortex images of isosceles A and B dots, for each L , one can see how the vortex configuration changes according to the geometry of the dots. At $L = 3$, for instance, three vortices in the isosceles A dot form a triangle pattern, which is elongated along the symmetry axis of the dot [Figs. 3(b) and 3(p)]. Meanwhile, a compressed triangle

pattern appears in the isosceles B dot [Figs. 3(i) and 3(w)]. If the expansion and compression of triangle patterns are disregarded, the vortex configuration is essentially unchanged. In other words, the configuration is stable with respect to the deformation of the dot shape. The situation is similar to other configurations observed at $L = 4$ [Figs. 3(c), 3(j), 3(q), and 3(x)], 6 [Figs. 3(e), 3(l), 3(s), and 3(z)], and 10 (not shown). Thus, we identify those vortex configurations (including $L = 1$) as “commensurate” states.

In other vorticities, vortices change their configurations according to the geometry. At $L = 5$, for instance, the vortex configuration in the isosceles A dot seems to be viewed as the combination of a $L = 3$ triangular pattern and a linear chain of two vortices [Figs. 3(d) and 3(r)]. Meanwhile, in the isosceles B dot, it seems to be constituted by two linear vortex chains [Fig. 3(k) and 3(y)]. The differences in vortex configurations between isosceles A and B dots are also noticeable at $L = 7$ [Figs. 3(f), 3(m), 3(t), and 3(aa)], 8 [Figs. 3(g), 3(n), 3(u), and 3(ab)], 9 (not shown), and 11 (not shown).

In Table I, we add vortex configurations observed in isosceles A and B dots using the nomenclature discussed above. For distinction, we append quotation marks in commensurate patterns in the isosceles dots since they are determined from the stability with respect to the geometric deformations, not by the (threefold axial) configuration symmetry. One can find that the commensurate vorticities in isosceles triangular dots (characterized only by “commensurate” patterns) are $L = 1, 3, 4, 6$, and 10, which coincide with those found in equilateral dots. Thus, the stability of vortex configurations against the geometric deformations leads to the same conclusion with respect to the commensurability in vortex states.

There are many coincidences in vortex configurations between equilateral and isosceles dots. Of particular importance are incommensurate states. At $L = 2$, $l2_{//}$ and $l2_{\perp}$ configurations respectively appear in isosceles A and B dots, while they appear as the ground and metastable states in equilateral dots. The situation is similar to $c4 + l3$ and $c3 + l4$ configurations at $L = 7$. At $L = 5$, equilateral and isosceles A dots share the same configuration of $c3 + l2$ as the ground state. More coincidences can be found in other incommensurate vorticities ($L = 8, 9$, and 11). Thus, vortex configurations found in isosceles triangular dots are intrinsically present in equilateral ones. These findings, together with the configuration symmetry found in isosceles triangular dots, provide strong support for the appearance of the twofold reflection symmetry in the incommensurate vortex configurations in equilateral triangular dots.

In summary, we have presented SQUID images of vortices in equilateral and isosceles triangular dots of weak pinning α -MoGe thin films for L up to 11. The observed images have

clearly shown the formation of pieces of a triangular lattice at triangular numbers of vortices, $L = 3, 6$, and 10 . These configurations, together with $L = 1$ and 4 configurations, have the threefold rotational symmetry and are essentially stable with respect to the deformations of the dot geometry, i.e., the transformation from equilateral triangles to two types of isosceles ones by reducing or expanding the height with respect to its base. Thus, we identified them as commensurate states. Meanwhile, for incommensurate states, vortex configurations vary sensitively with the geometric deformations. For each incommensurate L , the vortex configurations observed in isosceles triangular dots with different shapes differ from one another, and one of them (or sometimes both) coincides with what is observed in equilateral dots. It turns out that the twofold reflection symmetry characterizes the frustrated vortex configurations observed in both equilateral and isosceles dots. These findings provide not only a clear distinction between commensurate and incommensurate states, but also strong support for the appearance of the twofold reflection symmetry in frustrated vortex configurations in mesoscopic triangular dots.

N. K. acknowledges discussions with S. Okuma. This work was supported by JSPS KAKENHI Grant Numbers 23540416, 26287075, and 26600011, Nanotechnology Network Project of the Ministry of Education, Culture, Sports, Science and Technology (MEXT), and the Inter-university Cooperative Research Program of the Institute for Materials Research, Tohoku University (Proposal No. 14K0004).

References

- 1) R. C. Ashoori, H. L. Stormer, J. S. Weiner, L. N. Pfeiffer, S. J. Pearton, K. W. Baldwin, and K. W. West, *Phys. Rev. Lett.* **68**, 3088 (1992).
- 2) P. Leiderer, W. Ebner, and V. B. Shikin, *Surf. Sci.* **113**, 405 (1982).
- 3) K. Mangold, J. Birk, P. Leiderer, and C. Bechinger, *Phys. Chem. Chem. Phys.* **6**, 1623 (2004).
- 4) V. V. Moshchalkov, L. Gielen, C. Strunk, R. Jonckheere, X. Qiu, C. Van Haesendonck, and V. Bruynseraede, *Nature* **373**, 319 (1995).
- 5) A. K. Geim, I. V. Grigorieva, S. V. Dubonos, J. G. S. Lok, J. C. Maan, A. E. Filippio, and F. M. Peeters, *Nature* **390**, 259 (1997).
- 6) A. Kanda, B. J. Baelus, F. M. Peeters, K. Kadowaki, and Y. Ootuka, *Phys. Rev. Lett.* **93**, 257002 (2004).
- 7) T. Cren, D. Fokin, F. Debontridder, V. Dubost, and D. Roditchev, *Phys. Rev. Lett.* **102**, 127005 (2009).
- 8) V. A. Schweigert, F. M. Peeters, and P. Singha Deo, *Phys. Rev. Lett.* **81**, 127 (1998).
- 9) B. J. Baelus, L. R. E. Cabral, and F. M. Peeters, *Phys. Rev. B* **69**, 064506 (2004).
- 10) V. R. Misko, B. Xu, and F. M. Peeters, *Phys. Rev. B* **76**, 024516 (2007).
- 11) H. J. Zhao, V. R. Misko, F. M. Peeters, V. Oboznov, S. V. Dubonos, and I. V. Grigorieva, *Phys. Rev. B* **78**, 104517 (2008).
- 12) V. R. Misko, H. J. Zhao, F. M. Peeters, V. Oboznov, S. V. Dubonos, and I. V. Grigorieva, *Supercond. Sci. Technol.* **22**, 034001 (2009).
- 13) N. Kokubo, S. Okayasu, T. Nojima, H. Tamochi, and B. Shinozaki, *J. Phys. Soc. Jpn.* **83**, 083704 (2014).
- 14) H. T. Huy, M. Kato, and T. Ishida, *Supercond. Sci. Technol.* **26**, 065001 (2013).
- 15) L. F. Chibotaru, A. Ceulemans, V. Bruyndoncx, and V. V. Moshchalkov, *Phys. Rev. Lett.* **86**, 1323 (2001).
- 16) H. J. Zhao, V. R. Misko, F. M. Peeters, S. Dubonos, V. Oboznov, and I. V. Grigorieva, *Europhys. Lett.* **83**, 17008 (2008).
- 17) L. R. E. Cabral, and J. Albino Aguiar, *Phys. Rev. B* **80**, 214533 (2009).
- 18) K. Kadowaki, *Sci. Technol. Adv. Mater.* **6**, 589 (2005).

-
- 19) I. V. Grigorieva, W. Escoffier, J. Richardson, L. Y. Vinnikov, S. Dubonos, and V. Oboznov, Phys. Rev. Lett. **96**, 077005 (2006).
- 20) N. Kokubo, S. Okayasu, A. Kanda, and B. Shinozaki, Phys. Rev. B **82**, 014501 (2010).
- 21) T. Nishio, S. Okayasu, J. Suzuki, N. Kokubo, and K. Kadowaki, Phys. Rev. B **77**, 052503 (2008).
- 22) The magnetic field was applied at some temperatures (~ 12 K) above T_c , followed by cooling of the samples in the magnetic field to temperatures ($\sim 2.7 - 3.7$ K) far below T_c at which scanning SQUID measurements were carried out.